ADVANCED MATERIALS INTERFACES
Open Access
www.advmatinterfaces.de

Chitosan-*Graft*-Gelatin Hydrogel Containing Bromothymol Blue as a Food Spoilage Indicator for Intelligent Food Packaging

*Bahareh Farasati Far, Mehdi Jahanbakhshi, Leila Jameie, Asefeh Shojaei, Kimia Zarei, Parsa Taromi, Shima Jafarzadeh, and Yavuz Nuri Ertas**

A remarkable one-third of global food production is wasted, resulting in significant economic damage and escalating food insecurity. To address this sustainability challenge, freshness identification in food packaging using intelligent materials has gained traction. This work introduces a chitosan-*graft*-gelatin (CS-g-GEL) hydrogel, incorporating a pH-responsive dye, bromothymol blue (BTB), as a colorimetric freshness indicator to monitor the spoilage of chicken breasts. The successful formulation of the hydrogels is verified using FTIR, AFM, SEM, TGA, and ^{1}HNMR characterization techniques. At pH 5 and pH 7.4, the swelling capacity of the hydrogel is 790% and 470%, respectively. A rise in colony-forming units (CFU) from 5.5 on day 1–7.4 log CFU g^{-1} on day 7 indicate microbial activity, and the production of carbon dioxide due to deteriorating food freshness decreases the pH in the food package. Additionally, CO_2 concentrations rise from 3.2 on day 1–22.1 (% v/v) on day 7, while O_2 levels decreases from 23.8 to near 0.5 (% v/v) in the same period. The developed hydrogel is demonstrated to serve as a smart and visual indicator of food freshness and offers a new dimension in the use of intelligent materials toward a global challenge.

1. Introduction

In response to a growing need to provide fresh and safe food, smart packaging has emerged with intelligent indicators to inform consumers about the quality of the food.[1–4] The use of smart packaging as part of food packaging has the potential to be advantageous because it is capable of monitoring conditions in the packed product, such as spoilage, freshness, ripeness, bacterial activity, as well as other characteristics (such as storage conditions and transport).[5,6] The intelligent packaging has utilized several design elements, including radio-frequency identification as well as biological and chemical indicators, such as integrity or freshness indicators and time-temperature indicators.[7,8] Freshness indicators are based on the analysis of metabolites produced by microorganisms and are

B. F. Far, P. Taromi
Department of Chemistry
Iran University of Science and Technology
Tehran 1684613114, Iran

M. Jahanbakhshi
School of Chemical Engineering
College of Engineering
University of Tehran
Tehran 141556619, Iran

L. Jameie
Department of Chemistry
Isfahan University of Technology
Isfahan 8415683111, Iran

A. Shojaei
Department of Biochemical and Pharmaceutical Engineering
School of Chemical Engineering
College of Engineering
University of Tehran
Tehran 11155–4563, Iran

K. Zarei
Faculty of Pharmacy and Pharmaceutical Sciences
Tehran Medical Sciences
Islamic Azad University
Tehran 1916893813, Iran

S. Jafarzadeh
Centre for Sustainable Bioproducts
Deakin University
Waurn Ponds, VIC 3216, Australia

Y. N. Ertas
Department of Biomedical Engineering
Erciyes University
Kayseri 38039, Turkey
E-mail: yavuzertas@erciyes.edu.tr

Y. N. Ertas
Department of Technical Sciences
Western Caspian University
Baku AZ1001, Azerbaijan

The ORCID identification number(s) for the author(s) of this article can be found under https://doi.org/10.1002/admi.202400799

DOI: 10.1002/admi.202400799

frequently employed in intelligent food packaging systems.[9] Generally, freshness indicators detect metabolic products produced by microbial growth (e.g., CO_2, organic acids in food, total volatile basic nitrogen, or sulfur derivatives) and show an apparent color change, revealing the condition of the ingested food in the package[10] Recent research has shown that pH-sensitive dyes such as bromothymol blue, methyl red, and anthocyanin extracts serve as effective indicators of food freshness.[11–15] Hydrophilic films, such as cellulose-based papers or starch-based films, are typically used as a dye carrier for the generation of these indicators.[5,16] Due to dissolved target chemicals (e.g., volatile nitrogen compounds or CO_2) in water, colorimetric indicators work via pH change.[17] A carrier with low hygroscopicity or a limited moisture environment within a sealed package may diminish the sensitivity of the freshness indicator.[18]

Bromothymol blue (BTB) can be applied in intelligent food packaging as a pH-sensitive dye that helps in measuring food spoilage[19] This dye alters its color depending on the pH level, which makes it a perfect tool for determining the freshness of the food. When incorporated into the packaging materials, BTB would change color from blue to yellow as a result of increased acidity due to spoilage of food products. This real-time color change will provide a signal to the consumer, thereby promoting food safety and reducing food waste. Several studies established the use of the BTB in several food packaging. Cao et al., described an intelligent film for real-time meat freshness detection that is based on cassia gum and BTB-anchored cellulose fibers.[20] The intelligent films had a sensitive in situ response to triethylamine, with a highly visible color change from pale yellow to blue-green. The light yellow films changed to blue as the meat (pork or chicken) transitioned from a fresh to a subfresh state, thus demonstrating that the intelligent films can accurately indicate the freshness of meat products. To monitor the freshness of skinless chicken breasts by detecting food spoilage, Rukchon et al., developed an on-package indicator consisting of two groups of pH-sensitive dyes, one of which is a mixture of bromothymol blue and methyl red, while the other is a mixture of bromothymol blue, bromocresol green, and phenol red.[21] CO_2 was used as a spoilage metabolite, and trials on skinless chicken breast samples verified that the indicator response correlated with microbial growth patterns, thus enabling real-time monitoring of spoilage. To address the weakness of the color response of pH-sensitive dyes to target chemicals produced during food spoilage, highly hydrophilic or water-containing materials such as hydrogels have been proposed as a way of preparing indicators since humidity affects the dye's sensitivity and efficiency of color changes.

A hydrogel is a 3D network based on hydrophilic macromolecules capable of retaining a large amount of water.[22] Various techniques can be used to fabricate hydrogels, including polyelectrolyte complexation, ionic interaction, thermoreversible gelation, chemical grafting or cross-linking, and hydrogen bonding.[23–25] Due to their various advantages in biodegradability and biocompatibility, natural polymer-derived hydrogels are receiving more attention as a sustainable alternative to synthetic materials. Proteins and carbohydrates are natural polymers that form hydrogels. Chitosan (CS) is a polysaccharide derived from chitin, which has been shown to be a safe, non-toxic, biodegradable, and antibacterial agent.[26,27] By interacting with the negatively charged membrane of the microbial cell, the CS molecule can cause leakage of components from within the bacterial cell.[28] CS can be used in a wide variety of biological applications due to its synergistic effects when combined with different substances.[29,30] Proteins can be formulated with CS to improve their structural, morphological, and functional properties. The crosslinkers used in many commercial hydrogels are often costly.[31] Therefore, it is important to develop and use environmentally friendly and bio-based crosslinkers.[32] Gelatin (GEL) possesses excellent properties of being biocompatible, gelating, emulsifying, and adsorption characteristics and is obtained through collagen hydrolysis.[33] The gel-forming properties of gelatin make it widely used in the photography, cosmetics, and pharmaceutical industries. GEL, which can be easily dissolved in water, has many applications related to the food industry; it also plays an integral role in the functional and structural properties of the gel.

The role and significance of grafting in the creation of CS-g-GEL (chitosan-*graft*-gelatin) hydrogels are foundational to the formation and stabilization of the hydrogel structure. These hydrogels are formed through both chemical and physical cross-linking processes. Physical cross-linking relies on non-covalent interactions, such as hydrogen bonds and hydrophobic interactions, to form a 3D network, whereas chemical cross-linking creates covalent bonds between polymer chains, giving the hydrogel structural stability. In the case of CS-g-GEL, the overall properties of the hydrogel are a result of both types of interactions. In particular, the formation of the hydrogel is initiated by non-covalent physical interactions such as the hydrogen bonds between CS and ammonium ions. Covalent bonds between CS and formaldehyde, and between formaldehyde and GEL, also cross-link the material and turn the solution into a gel-like substance. The resulting hydrogel has a CS structure grafted with GEL molecules, which shows the importance of grafting in stabilizing and enhancing the functional properties of the hydrogel for various applications. The aim of this investigation was to develop a food packaging hydrogel involving GEL and CS and to assess the swelling characteristics of these materials at different pH levels. ^{1}HNMR, FTIR, and TGA measurements were utilized to determine the interactions between the components. Using FE-SEM and AFM analyses, the morphology of freeze-dried CS hydrogel cross-linked with GEL was examined. The produced hydrogel was then examined for its antibacterial activity and its capacity to monitor spoiling using indicator hydrogels, such as changes in CO_2 and O_2 concentrations and colony-forming units (CFU). The CS-g-GEL hydrogel was shown to be a useful material for intelligent food packaging as a food spoilage indicator.

2. Experimental Section

2.1. Chemicals and Materials

Chitosan with medium molecular weight (98% deacetylation) and gelatin (type A, from porcine skin, 300 g Bloom) were purchased from Sigma–Aldrich (St. Louis, MO, USA). Glacial acetic acid, aq. formaldehyde (37% in water), ammonia (25% in

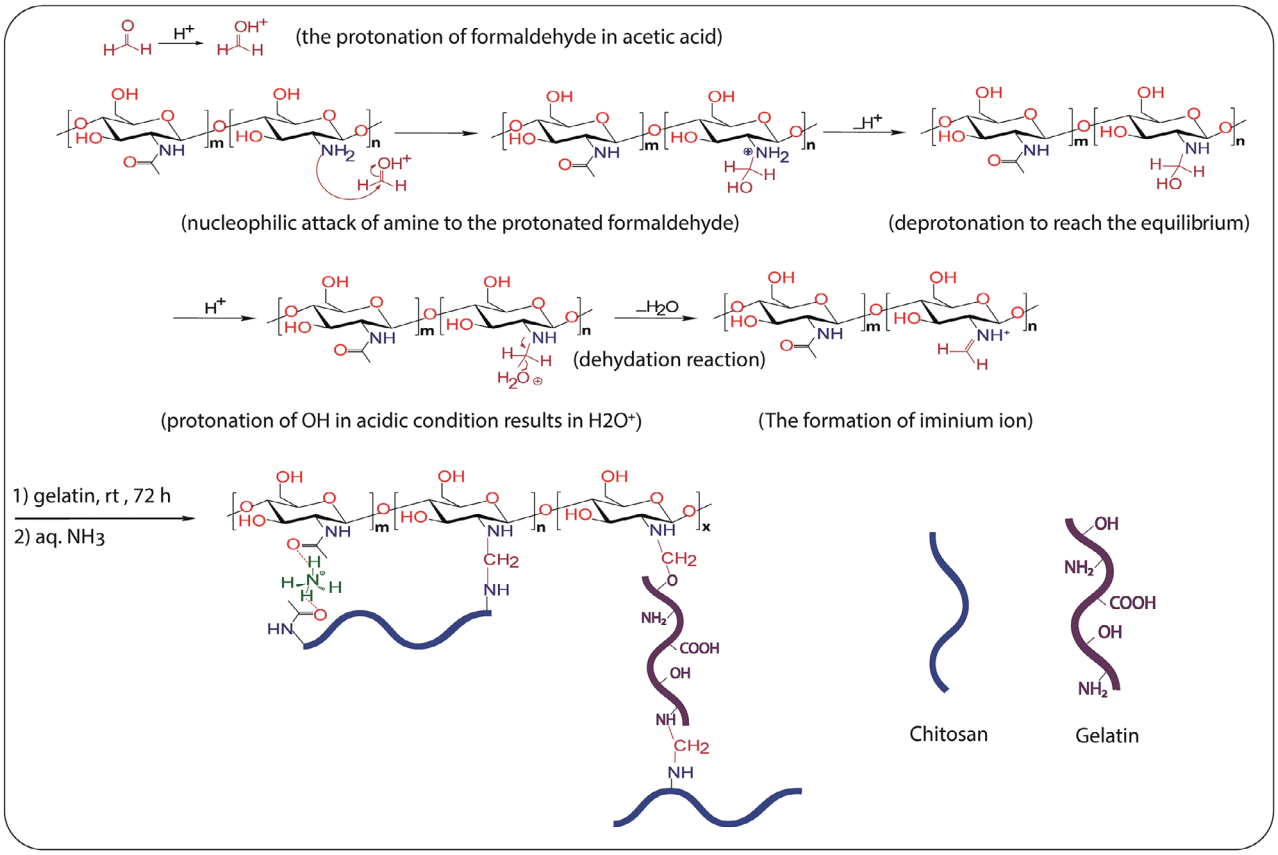

Figure 1. Synthesis pathway of the CS-g-GEL hydrogel.

water), aq. hydrochloric acid (37%), ethanol (96%), and methanol (≥99.9%) were obtained from Merck (Germany).

2.2. Synthesis Method

The process developed by Farasati Far et al., was modified to create the CS-g-GEL hydrogel.[34] To create a transparent CS solution, 1200 mg of CS was dissolved in 1% acetic acid solution (v/v) and thoroughly mixed with a magnetic stirrer for 8 h. The protonation process was then started by gradually adding 5 mL of 37% formaldehyde solution, which formed an iminium ion for 2 h, as shown in **Figure 1**. 500 mg of GEL was added to the CS solution for cross-linking. After that, a magnetic stirrer was used to agitate this mixture for an additional 48 h. A solution containing 25% ammonia was added to induce gelation, which caused the hydrogel to form quickly. Ethanol (96%) and methanol (≥99.9%) were used to wash the hydrogel with three replicates in order to remove any unbound or unreacted materials. The next step was vacuum filtration and drying in a 50 °C vacuum oven. CS-g-GEL hydrogel was immersed in the indicator water solution to prepare the indicator hydrogel. The indicator solution was developed by originally mixing BTB in aqueous ethanol (70%, v/v) to achieve a concentration of 0.25% (v/v), followed by dilution to 0.01% (w/v) with distilled water to create the indicator water solution. First, the pH of the indicator water solution was adjusted to 7, and then the hydrogel was immersed in the solution for 24 h. Once the dyed hydrogel had been removed, filter paper was used to dry the wet surface.

2.3. Characterization of Hydrogels

2.3.1. ^{1}H NMR Analysis

^{1}H NMR spectra were measured on an Avance Bruker DRX-500 spectrometer. Deuterium (D_2O) was used as the solvent, and the solvent signal was used for internal calibration. (D_2O): δ (1H) = 4.79 ppm.

2.3.2. Fourier Transform Infrared (FTIR) Analysis

Without further sample preparation, Fourier transform infrared (FTIR) spectra were obtained in transmission mode on an FT-IR spectrometer Agilent Cary 630 (Agilent Technologies/EUA).

2.3.3. Field Emission Scanning Electron Microscopy (FE-SEM) Analysis

Field emission scanning electron microscopy (FE-SEM) (Topcon/Singapore) was used to study the morphology of the CS-g-GEL. The samples were coated with a thin 16 nm gold film (Bal-Tec/USA).

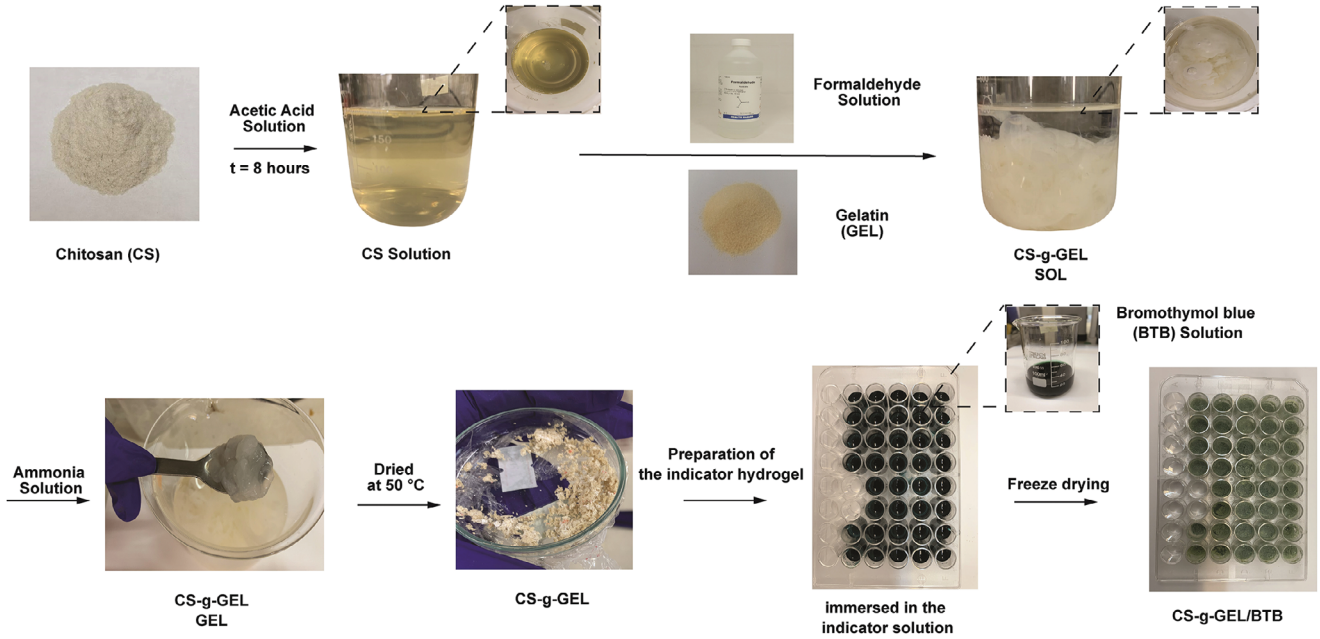

Figure 2. Schematic illustration of the formation of the CS-g-GEL and CS-g-GEL/BTB hydrogels.

2.3.4. Thermogravimetric Analysis (TGA) Analysis

TGA analysis was performed on an STA 449F3 Calorimeter (Netzsch/Germany) (Model TGA 50, Japan). This calorimetric experiment was performed at a heating rate of 10 °C min^{-1} under a nitrogen atmosphere over the following temperature ranges: 25–300 °C.

2.3.5. Atomic Force Microscopy (AFM) Analysis

Atomic force microscopy (AFM) was performed using a NanoScope E system manufactured by Digital Instruments (USA). The AFM analysis was conducted in contact mode.

2.4. Swelling Behavior of Hydrogels

CS-g-GEL/BTB hydrogel was prepared into 250 mg tablets to determine the swelling rate and the percent of water absorbed by the hydrogel. In order to assess the swelling behavior of CS-g-GEL/BTB hydrogel at various pH values (pH 5, pH 7.4), each CS-g-GEL/BTB hydrogel was stored in a buffer solution for 24 h at room temperature. This was followed by the removal of all excess water not incorporated into the hydrogel structure and the weighing of each interval of excess water. Dry hydrogels were immersed in buffer solution and weighed using Equation (1), where W_s and W_d are the swollen and dried weights, respectively (n = 3 for each data point). Also, equilibrium water content (EWC%) was calculated using Equation (2).

$$\text{Swelling ratio } (SR) = (Ws - Wi) / Wi \quad (1)$$

$$\text{Equilibrium water content } (EWC\%) = (Ws - Wd) / Ws \times 100 \quad (2)$$

where W_s and W_i are the weights of swollen and initial hydrogels, respectively.

2.5. Application of Indicator Hydrogel as Spoilage Monitor (CO_2, O_2, and Colony Forming Units Investigations)

A sterile glass vial was used for the storage of 3 g of fresh chicken breast. The indicator hydrogel, which had been prepared in the beginning, was placed on an aluminum shelf positioned above the meat, ensuring that there was no direct physical contact between the two items. The glass vial was sealed with PTFE rubber septa and kept in a refrigerator at a temperature of 4 °C for a duration of 7 days. The Mocon headspace analyzer (CheckMate 3, Dansensor, Denmark) was utilized in order to determine the degree to which the concentration of CO_2 and O_2 in the atmosphere of the sealed chicken sample changed over 7 days of storage. Plate counting was utilized in order to determine the total viable count of the bacteria that were present in the chicken meat. On predetermined storage days, a chicken sample weighing 3 g was moved to a glass flask that contained 20 mL of PBS. Subsequently, the mixture was agitated at a speed of 350 rpm for a duration of 10 min in order to achieve a uniform bacterial solution. A series of dilutions were made and then applied to the surface of the LB agar plates. The Petri dishes were subsequently placed in an incubator at a temperature of 37 °C for a duration of 24 h to facilitate the analysis of microorganisms. The bacterial counts were quantified as colony-forming units (CFU) per gram of chicken sample (CFU g^{-1}).

2.6. Assessment of Antimicrobial Activity of Hydrogels

The agar disk diffusion method was used to assess the hydrogel's antibacterial activity against gram-positive (*Staphylococcus aureus*)

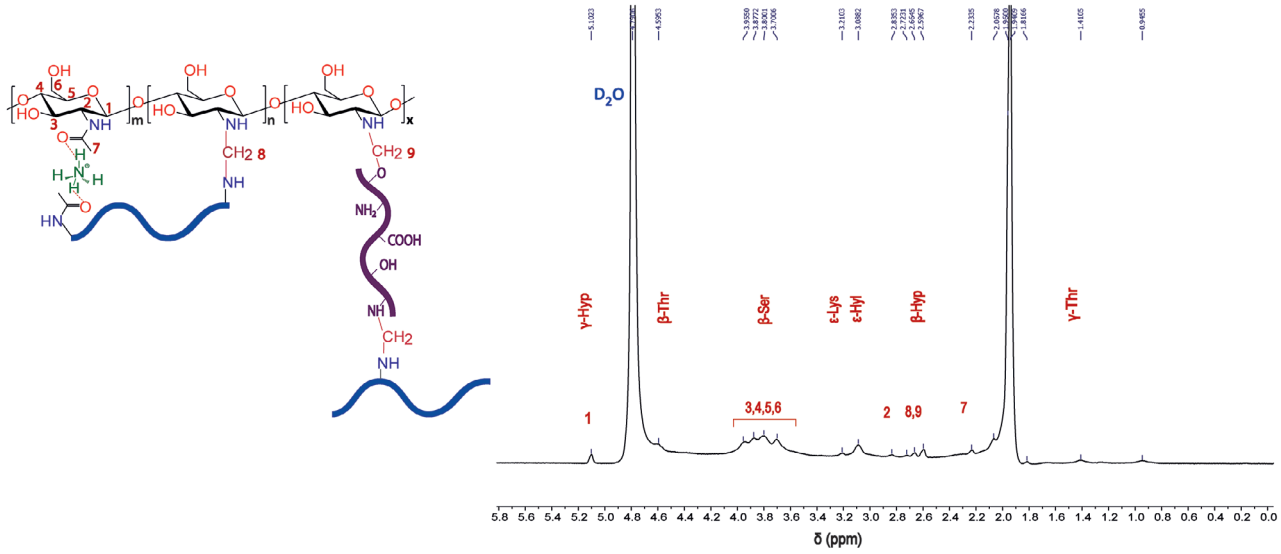

Figure 3. ^{1}HNMR spectrum of CS-g-GEL.

and gram-negative (*Escherichia coli*) bacteria.[35] The fresh target bacteria were cultured, and a diluent solution, such as physiological serum, was used to create a bacterial suspension with a concentration of 0.5 McFarland (equivalent to 1.5×10^8 CFU mL^{-1}). The bacterial suspension was diluted in order to reach the target cell count. Next, a sterile cotton swab was used to apply the bacterial suspension to the agar plate surface. The hydrogel samples (15 µL) were loaded onto the sterile discs' surface. The plates were incubated at 30 ± 5 °C for 48 h in a temperature-controlled incubator. Using a ruler or vernier caliper, the diameter of the growth inhibition zone encircling the discs was measured after incubation and recorded in millimeters. After three analyses of each bacterial strain, the mean values were determined.

2.7. Statistical analysis

Curve fitting and statistical analysis were carried out utilizing GraphPad Prism software, version 8 (GraphPad Software, Inc., USA (San Diego, CA). The means ± standard deviations were used to represent the data from three separate experiments. A one-way analysis of variance was used to determine statistical significance after the data sets' homoscedasticity and normality were confirmed. The predetermined level of statistical significance for each analysis was $p = 0.05$.[36]

3. Results and Discussion

3.1. Synthesis Mechanism of CS-Based Hydrogels

There are several ways to create CS-based hydrogels, including chemical and physical cross-linking processes.[37] Chemical cross-linking creates covalent bonds between polymer chains to give structural stability,[38] whereas physical cross-linking depends on non-covalent interactions between polymer chains, such as hydrogen bonds and hydrophobic interactions, to form a 3D network.[39] The mechanisms by which CS-g-GEL hydrogel was formed in this study were non-covalent physical interactions (hydrogen bonds between CS and ammonium ions) and covalent bonds between CS and formaldehyde and formaldehyde with GEL. The attachment of GEL to CS is shown in Figure 1. Figures 1 and 2 depict the CS-g-GEL hydrogel design approach. The first step in the procedure is to prepare a CS solution, which is then protonated in an acidic environment. This is accomplished by subjecting the amine groups in the CS to an acid—usually acetic acid—which causes the amine groups to acquire a positive charge.[40] Following protonation, formaldehyde is added to the CS. Iminium ions, a particular kind of stabilized cation, are created when the formaldehyde combines with the protonated amine groups. This process, which is also known as the formation of a Schiff base, involves the loss of a water molecule.[41] The mixture is then supplemented with GEL, which contains reactive compounds. The iminium ions on the backbone of the CS undergo a reaction with the reactive compounds present in the GEL. This is an important step because it causes the CS chains to cross-link, which turns the solution into a gel-like substance.[28,42] At room temperature, the cross-linking reaction is facilitated over time. Finally, an ammonia solution is added to finish the hydrogel formation. The hydrogel matrix is further stabilized, and the surplus hydrogen ions are probably neutralized by the ammonia. The end product is a hydrogel in which the CS structure was grafted with molecules of GEL. Farasati Far et al., used this economical and bio-based technique to create antibacterial and antioxidant pads using chitosan-*graft*-pomegranate extract hydrogel.[32]

3.2. Characterization of Hydrogels

3.2.1. ^{1}HNMR Analysis

In order to investigate the CS-g-GEL hydrogel, ^{1}H NMR spectroscopy was conducted in D_2O. The zone of the proton peaks

Table 1. ^{1}HNMR Characteristic proton of the amino acids of GEL.

Characteristic Proton of the Amino Acids of GEL	Chemical Shifts Before Grafting [ppm]	Chemical Shift After Grafting [ppm]
γ-threonine (γ-Thr)	1.2	1.3
β-threonine (β-Thr)	4.3	4.48
β-serine (β-Ser)	3.9	3.8
ϵ-hydroxylysine (ϵ-Hyl)	3	2.95
ϵ-lysine (ϵ-Lys)	3	2.95
γ-hydroxyproline (γ-Hyp)	4.6	4.98
β-hydroxyproline (β-Hyp)	2.4	2.47

for pure CS was reported at 4.6 ppm (H1 of the glucosamine ring), 3.1 ppm (H2 of the glucosamine ring), and within the range of 3.1–3.8 ppm (H3, H4, H5, H6).[43] As shown in **Figure 3**, the acetyl group (—CH_3) is responsible for the signal at 1.960 ppm, whereas the H2 proton associated with CS is responsible for the signal at 2.835 ppm. According to a study, the signal at 2.835 ppm in CS is caused by the proton H2, whereas the acetyl group may be in charge of the chemical shifts at 1.960 ppm.[41] CS has chemical shifts ranging from 3.70 to 4.00 ppm corresponding to H3–H6 protons. Chemical shifts between 3.43 and 4 ppm are caused by CS protons.[28] As a result of the cross-linking of gelatin and chitosan, methylene groups are formed at a frequency of 2.596 ppm (H8, H9). A signal in the range of 5.102 ppm is produced by hydrogen bonding to anomeric carbon (H1). According to **Table 1** and Figure 3, typical peaks of amino acids were previously reported in ^{1}H-NMR analysis of GEL (γ-threonine, γ-Thr), β-threonine (β-Thr), β-serine (β-Ser), ϵ-Hydroxylysine (ϵ-Hyl), ϵ-Lysine (ϵ-Lys), γ-hydroxyproline (γ-Hyp) and β-hydroxyproline (β-Hyp).[44] The characteristic peaks of amino acids were shifted after GEL was grafted into CS, demonstrating the grafting process.

3.2.2. FTIR Analysis

Figure 4a displays the FTIR analysis of CS, GEL, CS-g-GEL, and CS-g-GEL/BTB hydrogels. The CS spectrum displays specific peaks at 974 cm^{-1} (C—O stretching), 1026 cm^{-1} (C—O—C stretching), 1072 cm^{-1}, and 1152 cm^{-1} (C—O stretching). Additionally, amides I and III exhibit absorption bands at 1642 and 1363 cm^{-1}, respectively. There is also a broad peak at 3345 cm^{-1} due to NH symmetric vibrations in the amino group.[42] The FTIR spectrum of the pure gelatin show that the peaks at 3450 and 3423 cm^{-1} were due to N—H stretching of secondary amide, C═O stretching at 1680 and 1640 cm^{-1}, N—H bending between 1550 and 1500 cm^{-1}, N—H out of plane wagging at 670 cm^{-1} and C—H stretching at 922 and 2850 cm^{-1}. The characteristic peak of the collagen fold in 3360 cm^{-1} is absent in the spectrum, which indicates the denaturation of collagen to produce gelatin. There is a broad peak at 3350 cm^{-1} associated with stretching vibrations between N—H and O—H. The bands at 1005–1020 cm^{-1} may correspond to absorptions caused by C—N stretching. There is an absorption band at 1657 cm^{-1} associated with the N-acetyl groups (C═O stretching of amide I), and a characteristic peak at 1561 cm^{-1} associated with the N—H bending. There is a peak at ≈1397 cm^{-1} (C—O—R), which represents the chemical crosslinking between GEL and CS. For CS-g-GEL/BTB, O—H stretching vibration bands enhanced due to the interaction of the hydroxyl group in BTB with the amine groups in CS, the intensity of the peaks for C—H, C—O—C, and C—C increased, and the enhanced band at 1726 cm^{-1} attributed to C═O vibrations appeared. Also, sulfonate stretching can be seen ≈1350–1470 cm^{-1} after dying hydrogel with BTB dye.

3.2.3. Rheological Properties

Figure 4b shows the rheological properties of the CS-g-GEL hydrogel at different shear rates and shear stresses. At very low shear rates (0.01 1/s), the hydrogel shows a high viscosity of 38600 (Pa.s), which depicts that the hydrogel is highly viscous and in a gel-like state. This implies that the material is non-Newtonian, especially showing shear-thinning behavior due to the rapid reduction in the viscosity as the shear rate rises. This property enables the hydrogel to respond uniformly to mechanical stress, which is of significance in instances such as that of food spoilage indicators. Thus, at the shear rates of ≈1 (1/s), the viscosity is equal to 13100 (Pa.s), and as the shear rates increase, the viscosity further decreases and is equal to 105 (Pa.s) when the shear rates are 1000 (1/s). These observations indicate that the hydrogel is capable of shifting from one mechanical state to another while retaining its functionalities, based on the applied shear rates. This characteristic of having high viscosity at low shear rates and shear thinning behavior guarantees that a uniform layer of the hydrogel is formed for tracking food spoilage. The reduction in viscosity under shear guarantees that the hydrogel responds sufficiently to physical interactions like handling and packaging and does not lose its structural and functional characteristics. This makes the CS-g-GEL hydrogel ideal for smart food packaging systems where it is necessary to continuously check for spoilage markers such as the pH level. CS hydrogels exhibit shear-thinning behavior, meaning their viscosity decreases with an increasing shear rate.[45,46] A study on the rheological behavior of dual network hydrogels of acrylamide and sodium alginate showed similar shear thinning behavior; the viscosity of the hydrogel decreased roughly with the increase in the shear rates.[47] This behavior guarantees that the hydrogel will not self-demolish as a result of mechanical stresses, which comes in handy in instances such as food spoilage sensors.

3.2.4. Thermogravimetric Analysis (TGA) Analysis

A thermogravimetric analysis was conducted to evaluate the thermal characteristics of the CS-g-GEL hydrogel. Two steps in the weight loss of the CS-g-GEL hydrogel were observed according to the TGA curve. During the initial region until 132 °C, a weight loss of 8.16% is attributed to the physical adsorption of water. As for the second weight loss step, which accounts for 78% of the weight loss of the CS-g-GEL (132–600 °C), thermal decomposition of the hydrogel bonds as well as the pyranose ring of the CS take place (Figure 4c). There were two phases of weight loss for CS. The initial phase begins at a temperature of 60 °C,

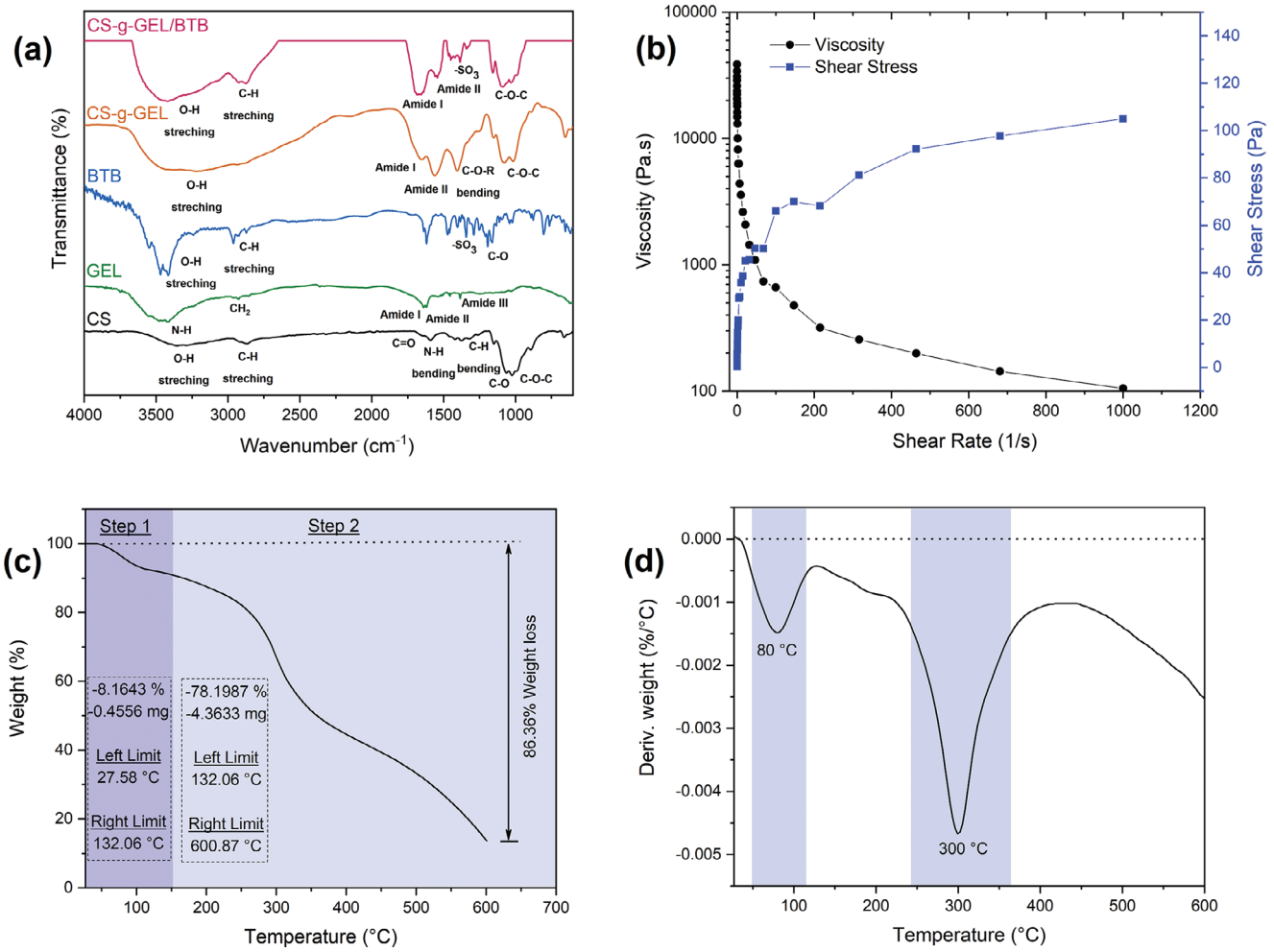

Figure 4. a) FTIR spectra of CS, GEL, CS-g-GEL, and CS-g-GEL/BTB. b) The flow curve of viscosity, c) TGA, and d) DTG of CS-g-GEL hydrogel.

which results in a mass reduction of 10%. The second stage initiates at 240 °C, achieving a peak at 380 °C, leading to a weight reduction of 41.4%. At ≈318 °C, GEL began to lose weight as a result of protein chains and peptide bonds breaking. For CS-g-GEL, the second stage starts at 132 °C and peaks at 300 °C, showing that CS-g-GEL changes the decomposition temperatures compared to pure CS and GEL. In a study, the TGA curve of chitosan-g-glycerol and carboxymethyl chitosan-g-glycerol hydrogels showed weight loss at 230–600 °C due to the thermal decomposition of the pyranose ring of chitosan and polymer structure degradation.[34] Differential thermogravimetry (DTG) was also used to determine the CS-g-GEL hydrogel (Figure 4d). Using DTG analysis, it was also confirmed that CS-g-GEL degrades in two steps between 27 and 600 °C. At 30 °C, the main decomposition peak for CS-g-GEL can be seen on the DTG curve. The maximum degradation of both CS and GEL occurs ≈300 °C. Because of the crosslinking of GEL with CS, TGA thermograms and DTG curves indicate that the thermal stability of CS-g-GEL is higher than that of CS. These results are in excellent agreement with those suggested by Jridi et al., that combining GEL and CS in a 50/50 ratio can enhance the physico-chemical properties of CS.[48]

3.2.5. Morphological Properties

The morphology of freeze-dried CS hydrogels crosslinked with GEL is shown in **Figure** 5a. CS-g-GEL hydrogel exhibits high porosity, crosslinking, and 3D structure. Crosslinked networks may lead to interconnections in CS-g-GEL hydrogel. In addition, water is absorbed by the hydrophilic sites of hydrogels during freeze-drying, making them porous. CS-g-GEL hydrogel can swell as a result of its porous structure, decreasing resistance caused by the flow of water. Figure 5b appears to have a denser network with a more compact and intertwined structure compared to Figure 5a, which may be due to the possible interaction of BTB with CS-g-GEL hydrogel.

The EDX spectrum of CS-g-GEL hydrogel is comprised of carbon (C) (51.17 wt.%), nitrogen (N) (20.21 wt.%), and oxygen (O) (28.62 wt.%) (Figure 5c). This composition is characteristic of CS and GEL, which consist of these elements mainly because of their polysaccharide and protein nature. The elemental composition of the hydrogel is slightly different due to the presence of BTB in the CS-g-GEL/BTB hydrogel. The elemental analysis shows that the ratio of carbon, nitrogen, oxygen, sulfur, and bromine in CS-g-GEL/BTB hydrogel is 39.42 wt.%, 27.61 wt.%, 30.27 wt.%,

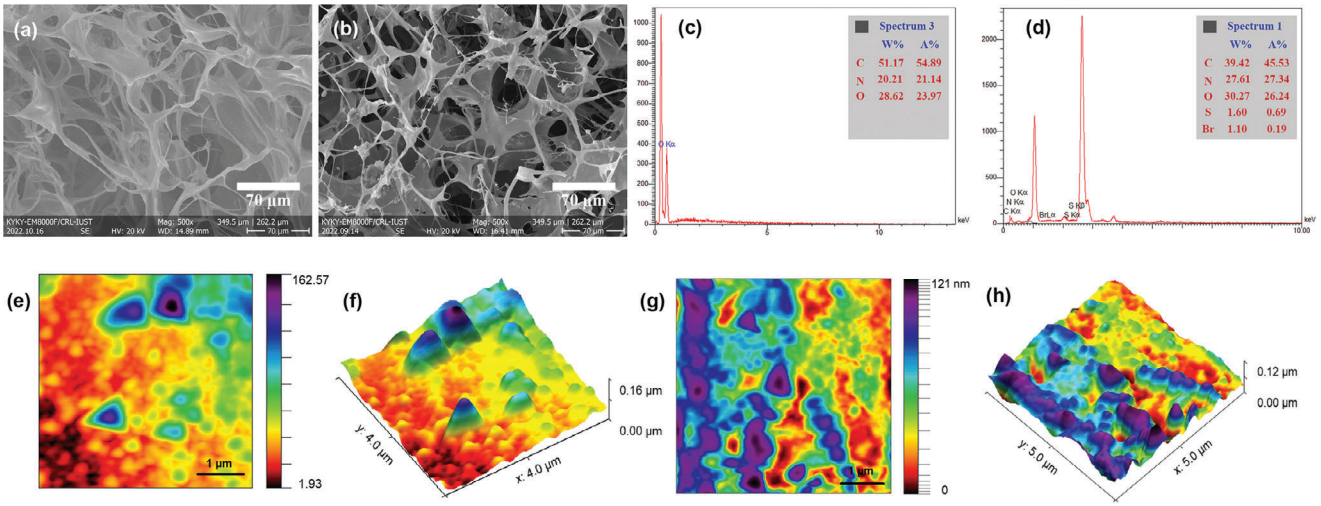

Figure 5. FESEM cross-sectional images of a) CS-g-GEL and b) CS-g-GEL/BTB hydrogel, EDX analysis of c) CS-g-GEL and d) CS-g-GEL/BTB hydrogel, and e,f) 2D and 3D AFM images of CS-g-GEL hydrogel and g,h) CS-g-GEL/BTB hydrogel.

1.60 wt.%, and 1. 10 wt.%, respectively (Figure 5d). The peaks corresponding to sulfur and bromine are evident, which confirms the presence of BTB in the hydrogel, thus suggesting successful loading of BTB into the matrix.

The AFM images present quantitative information on the surface characteristics of these hydrogels. The color scale of height is used in the 2D image CS-g-GEL, where high areas are represented in blue and low areas in red. The 3D image gives enhanced details about the roughness and texture of the surface, showing the raised features and the difference in height of up to 162 (Figure 5e,f). The 2D image of the CS-g-GEL/BTB reveals phase height differences in the range of 121 nm, which is further illustrated in its 3D image (Figure 5g,h). The surface of CS-g-GEL hydrogel seems to be rougher, which may imply that it is more irregular than the other samples. CS-g-GEL/BTB hydrogel has comparatively low roughness values, which indicates that the surface of the hydrogel is smoother. CS-g-GEL hydrogel has higher peaks, up to ≈162 nm. However, CS-g-GEL/BTB hydrogel exhibits significantly smaller peaks of up to 121 nm.

3.2.6. Swelling Properties

The swelling ratio of the CS-g-GEL/BTB hydrogel was determined by immersing the hydrogel in distilled water (pH 7.4) and buffer at pH 5. **Figure 6** illustrates the effects of pH levels on the swelling ratios of CS-g-GEL/BTB hydrogel in relation to time. There are three types of covalently cross-linked CS based on the structure of their polymer chains: CS cross-linked to itself, hybrid polymer networks (HPNs), and semi- or fully interpenetrating polymers.[49] In this study, physical entanglements and covalently cross-linked chemical interactions in the presence of GEL played an essential role in the formation of CS-g-GEL/BTB hydrogel. Therefore, crosslinking leads to a structure that contains many pores that can be filled with water and BTB. The swelling ratio of CS-g-GEL/BTB hydrogel typically changes at different pH values. A change in pH can affect the swelling ratio by protonating and deprotonating functional groups. Because CS's primary amine has a pKa of 6.5, the amines in the polymer chain are positively charged (NH_3^+) when the pH in the solution is lower than 6.5, resulting in swelling. In a study, the swelling ratio of a CS-diethyl malonate hydrogel was examined, revealing that the hydrogel demonstrated a swelling ratio of ≈600% at pH = 7.4 after 24 h, underscoring its ability to absorb water and expand under pH = 7.4.[50] Additionally, the equilibrium water content of CS-g-glycerol hydrogel exhibited EWC value of 97% at 7.4 after 24 h.[34]

3.3. Indicator Hydrogel and CO_2 Response

As a dye pH indicator, BTB is incorporated into the indicator hydrogel, which changes color from blue to yellow as the pH drops. An indicator solution with different pH values demonstrated a visual color difference (**Figure 7a**). The color changed to yellow when the pH level reached 3. A blue color was observed as the pH reached 12. The BTB-dye pH indicator was carried upon a CS-g-GEL hydrogel, which also served as an adsorbent for CO_2. Due to the presence of a high amount of water in the network of the hydrogel, it serves as a reservoir in which CO_2 dissolves and forms carbonic acid, causing a visible change in the color of the dye pH indicator incorporated in the hydrogel (Figure 7b). Because CO_2 dissolves rapidly and proton generation occurs quickly, the indicator hydrogel changes color more rapidly and more sensitively than ordinary indicators. The UV–vis absorption spectra of BTB consist of several peaks, which change with the change in pH (Figure 7c,d). At reduced pH values, the absorption maxima are found at shorter wavelengths, and that represents the protonated form of the dye (Figure 7e). Deprotonated forms are represented in a new position toward longer wavelengths as the pH level increases. At pH 3.5, it is possible to note the significant increase at ≈450 nm, after which the intensity of the peak gradually reduces up to ≈615 nm with an increase in pH. The changes between these pH levels are not as drastic as the acidic range, but they are visible, especially the peak at ≈615 nm rises with increasing pH. These changes in the absorption spectra of BTB with the changes in pH make it ideal for use when showing changes in pH in its

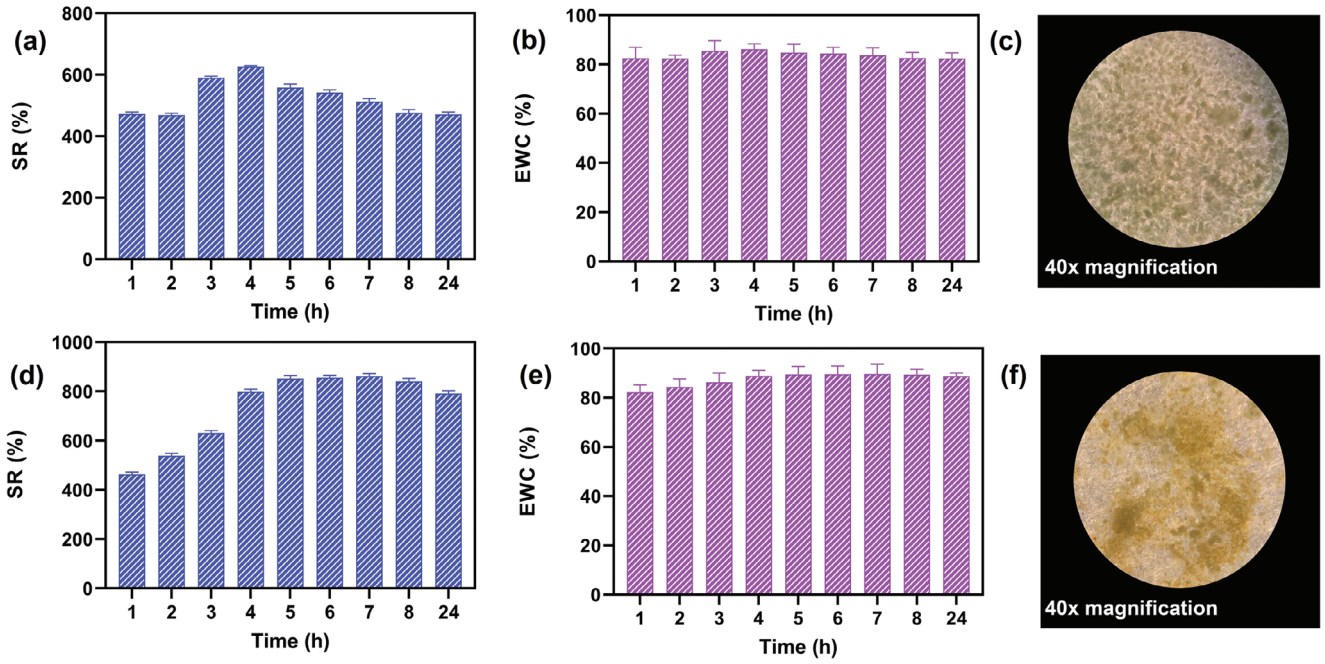

Figure 6. a–c) SR (%), EWC (%), and optical microscopic images of swelling of CS-g-GEL hydrogel at pH 7.4. d–f) SR (%), EWC (%), and optical microscopic images of swelling of CS-g-GEL hydrogel at pH 5.

different uses in applications such as intelligent food packaging showing spoilage through change in color.

3.4. Correlation of the Indicator Hydrogel Response to Chicken Breast Freshness

The freshness of chicken breasts quickly decreases with time, even when stored at 4 °C. Chicken meat spoilage is generally attributed to microorganisms as well as the production of CO_2 and basic nitrogen gases (e.g., trimethylamine, ammonia, dimethylamine) by microbes.[21] This means that changes in CO_2 levels inside the chicken meat packaging can be used to indirectly monitor the freshness of chicken meat.[51] It was worth exploring the possibility of using the prepared indicator hydrogel as a freshness indicator since it proved to be sensitive to CO_2 and showed color changes related to its CO_2 levels. Figure 7f–h illustrate the application of a freshness indicator produced from the hydrogel to packaged chicken breasts. A separate chamber inside the package was designed to place the pH-responsive dyes away from the packed food since the dye is not food contact-grade dye. Following 2 days of the addition of fresh chicken to the indicator hydrogel, the hydrogel quickly changed color from green to green-yellow, signaling that CO_2 was being generated. A noticeable color change was noticed after 3 days at 4 °C, suggesting that it can be used in intelligent packaging. In order to fabricate a robust hydrogel-based indicator, the effect of temperature, the limited level of CO_2 detection, and color persistence require further investigation. The meat has an off odor as well as a high level of CO_2 after the third day. On this day, the indicator hydrogel displayed a yellow color in agreement with its high CO_2 content, indicating it is useful for detecting spoilage of chicken meat.

3.5. Indicator Hydrogel and CO_2 Response

Figure 8 displays the colony-forming units (CFU), CO_2 production, and O_2 consumption of packaged chicken breasts over 7 days. A schematic illustration of the colony-forming units analysis procedure is shown in Figure 8a. The log CFU/g increases from day 1 to day 7, indicating a higher CFU count during the middle of the incubation period. Days 1 and 3 show a slightly higher increase compared to day 2, while day 4 subsequently increases sharply, showing microbial growth and spoilage period (Figure 8b,c). The concentration of CO_2 (%V/V) continues to rise progressively during 7 days and reaches a level of <5% on the first day and 25% on the seventh day (Figure 8d,e). The increase in CO_2 levels is proportional to microbial action and metabolic activity within the packaged chicken. On the other hand, the O_2 levels measured in % V/V significantly reduced from day 1 to day 7. O_2 levels at the beginning of the experiment were ≈21% on day 1, then dropped due to the consumption of O_2 by the aerobic microorganisms (Figures 8f,g). O_2 levels were almost nonexistent on the 7th day. The decrease is shown on the heat map chart (f), where the colors gradually change from warm to cool. These changes regarding the most important metabolites, such as CFU, CO_2, and O_2, are effective markers for spoilage as well as the efficiency of the CS-g-GEL/BTB hydrogel for monitoring chicken breast freshness spotting. Using the absorbent BTB dye that alters color with a change in pH due to CO_2 production, spoilage can be detected. Kim et al., prepared a bromocresol purple dye-based pH-responsive indicator and stored chicken breast samples at 4 and 10 °C, and pH values were measured using a pH meter. The pH was initially stable and low (pH 5.9–6.0), indicating fresh chicken. The pH increased slightly to 6.1 at 4 °C and was constant for 6 days, then rose sharply. The pH of the sample increased

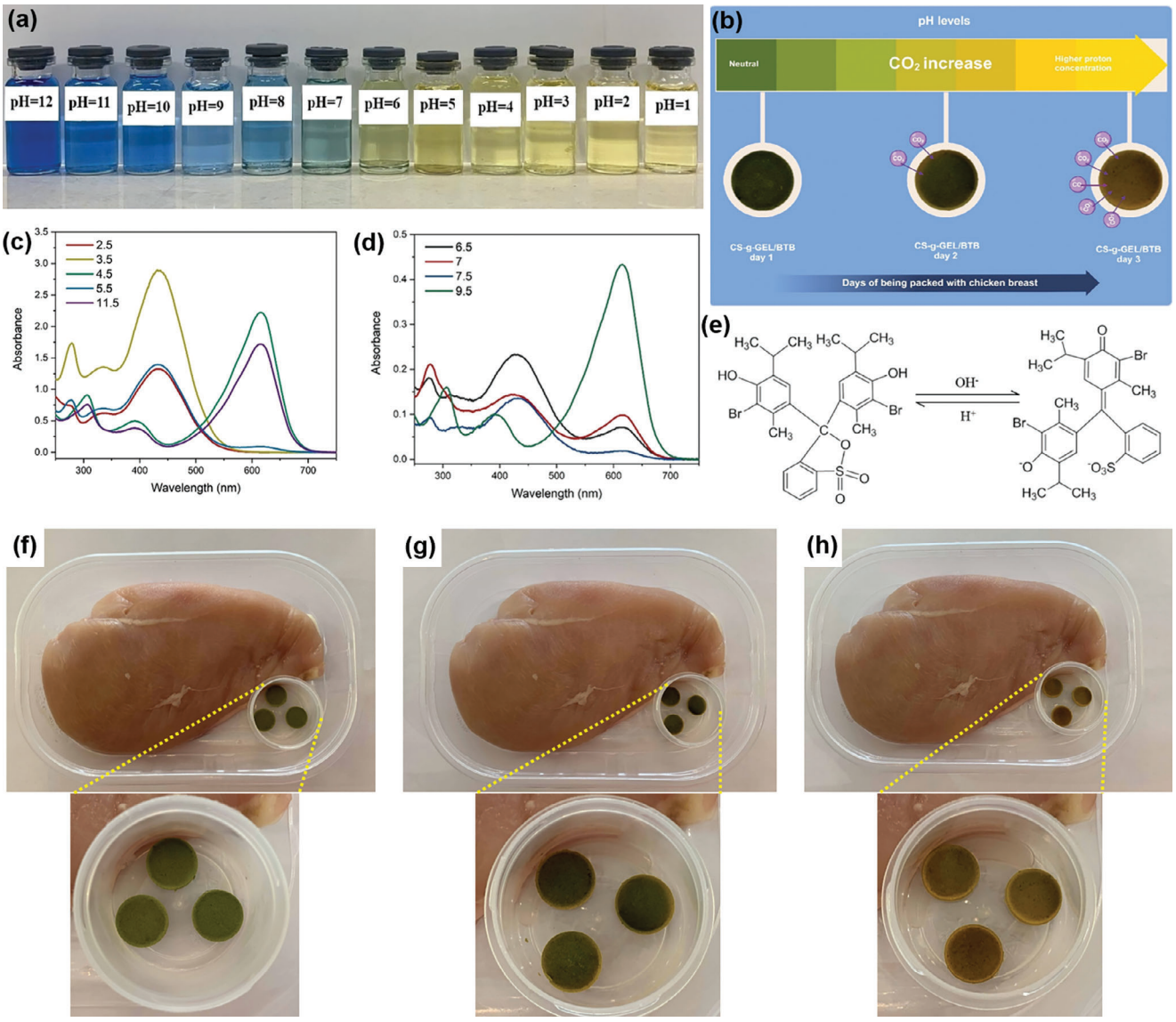

Figure 7. a) A comparison of BTB color changes in response to pH, b) color of CS-g-GEL/BTB hydrogel after being packed with chicken breast, c,d) the influence of pH on the absorption spectrum of the indicator solution, e) changes in BTB structure in acidic and alkaline solutions, and f) color of CS-g-GEL/BTB hydrogel with chicken breast in 1, g) 2, and h) 3 days at 4 °C.

steadily and linearly at 10 °C and reached a value similar to that of the 6-day sample stored at 4 °C after 3 days.[52] Physicochemical and microbiological deterioration of chicken quality was linked to the change in pH. They explained that the start of deterioration is indicated by a pH range of 6.3–6.5, with increased pH due to the accumulation of trimethylamine and other volatile basic nitrogen compounds from microbial activity. They reported that fast spoilage is signaled by rapid pH increases and is correlated with the total viable count. In another study, Lu et al., developed sugarcane bagasse nanocellulose hydrogel containing bromothymol blue/methyl red, and the hydrogel color changed to orange–yellow after 24 h and then to bright red after two days of storage at 4 °C, indicating a high level of CO_2.[53] The study also examined the CO_2 emission by putting chicken samples with the hydrogel in closed containers; the color of the hydrogel changes with the CO_2 concentration. This was accompanied by increased microbial counts (CFU) during storage. Microbial counts and CO_2 levels were highest on day four, while oxygen was completely consumed by the end of the week.

3.6. Antibacterial Activity

CS-g-GEL and CS-g-GEL/BTB hydrogels were tested for antibacterial activity using the agar disk diffusion method. The CS-g-GEL hydrogel had a higher antibacterial activity when it was tested against *Escherichia coli* ATCC 11775 and *Staphylococcus aureus* ATCC 12600 ($p = 0.0036$) (**Figure 9**a). As a result of CS and GEL being present in the CS-g-GEL hydrogel, considerable antibacterial activity was observed. CS-g-GEL hydrogel

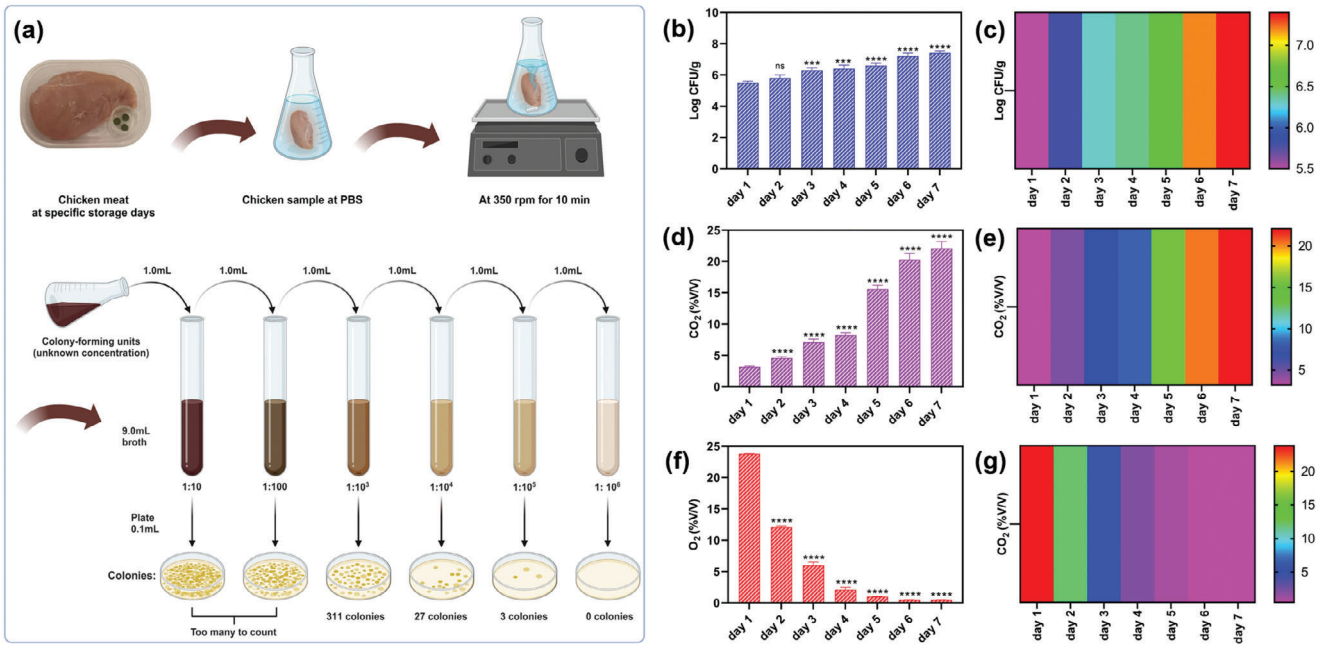

Figure 8. a) Schematic illustration of the colony-forming units analysis procedure. The colony-forming units b,c), carbon dioxide d,e) production, and oxygen f,g) consumption of packaged chicken breasts over seven days. (For all charts, $^{****}p < 0.0001$; $^{***}p < 0.001$; $^{**}p < 0.01$; $^{*}p < 0.05$).

demonstrated inhibition zones of 12 ± 1 mm and 9 ± 1 mm against *Escherichia coli* ATCC 11775 and *Staphylococcus aureus* ATCC 12600, respectively (Figure 9b). CS ($-NH_3^+$) is reported to interact negatively with bacterial cell walls due to its positively charged amino groups, which eventually disrupts cell respiration, mitosis, and bacterial viability.[54,55] CS-g-GEL/BTB hydrogel did not show antibacterial activity against *Escherichia coli* and *Staphylococcus aureus* (Figure 9c,d). BTB itself does not have inherent antibacterial activity. It is primarily used as a pH indicator and could potentially alter the chemical environment of CS. The interaction between BTB and CS could interfere with the protonation of chitosan's amino groups, which are essential for its antibacterial properties. This interference could diminish the effectiveness of CS in disrupting bacterial membranes. In other words, while CS is active in its natural form, its antibacterial function may be diminished when it is embedded in a matrix that alters its structure or environment, like with BTB.

4. Conclusion

It is important to consider freshness when consuming and storing products. Using a colorimetric freshness indicator, chitosan-graft-gelatin (CS-g-GEL) hydrogel was prepared to monitor the spoilage of chicken breasts. It was confirmed through FTIR, AFM, SEM, TGA, and 1HNMR characterization that the hydrogel was successfully formulated. According to the colorimetric freshness test, the freeze-dried powder exhibited 790% and 470% swelling capacity at pH 5 and pH 7.4. The SEM images of the prepared hydrogel revealed a porous structure, indicating that crosslinking was successful. Antibacterial activities of CS-g-GEL hydrogel were observed against both Gram-positive and Gram-negative bacteria. There was no evidence of antibacterial activity in the CS-g-GEL/BTB hydrogel because BTB does not exhibit any antibacterial properties. Color changes of the pH indicator were clearly visible at various pH levels (pH 1–10). After three days at

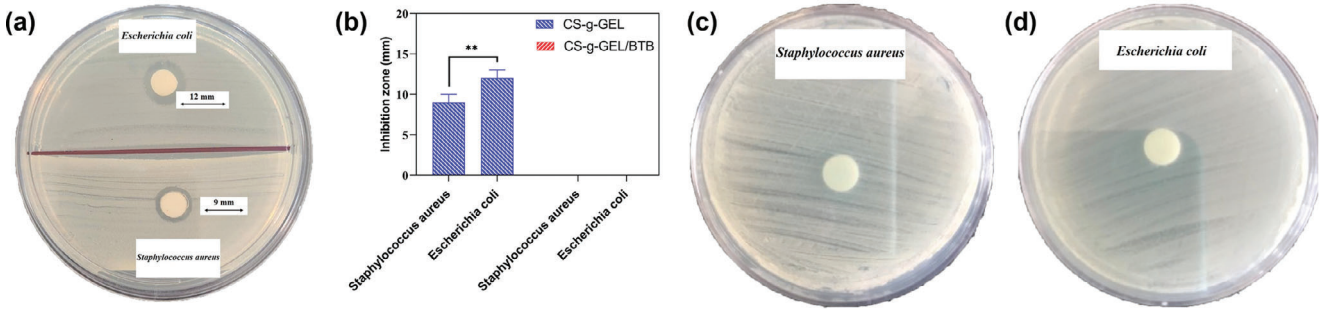

Figure 9. Antibacterial inhibition zone for CS-g-GEL hydrogel against a) Staphylococcus aureus ATCC 12600 and Escherichia coli ATCC 11775 bacteria. b) Comparison of antibacterial inhibition zones for CS-g-GEL and CS-g-GEL/BTB hydrogel. c,d) Antibacterial inhibition zone for CS-g-GEL/BTB hydrogel against Staphylococcus aureus ATCC 12600 and Escherichia coli ATCC 11775 bacteria.

4 °C, indicator hydrogel exhibited a noticeable change in color, suggesting it could be utilized for intelligent packaging.

Acknowledgements

M.J. and L.J. contributed equally to this work.

Conflict of Interest

The authors declare no conflict of interest.

Data Availability Statement

The data that support the findings of this study are available from the corresponding author upon reasonable request.

Keywords

chitosan, color change, food freshness, food spoilage indicator, smart packaging

Received: October 7, 2024
Revised: December 27, 2024
Published online:

[1] X. Yao, J. Liu, H. Hu, D. Yun, J. Liu, *Food Hydrocolloids* **2022**, *124*, 107305.
[2] J. Kan, J. Liu, F. Xu, D. Yun, H. Yong, J. Liu, *Food Hydrocolloids* **2022**, *124*, 107293.
[3] M. Ferri, K. Papchenko, M. Degli Esposti, G. Tondi, M. G. De Angelis, D. Morselli, P. Fabbri, *Acs Appl Mater Inter* **2023**, *15*, 28594.
[4] Z. L. Yu, V. Boyarkina, Z. Y. Liao, M. S. Lin, W. C. Zeng, X. A. Lu, *Acs Food Sci Technol* **2023**, *3*, 199.
[5] S. Kalpana, S. R. Priyadarshini, M. Maria Leena, J. A. Moses, C. Anandharamakrishnan, *Trends Food Sci. Technol.* **2019**, *93*, 145.
[6] M. Cvek, U. C. Paul, J. Zia, G. Mancini, V. Sedlarik, A. Athanassiou, *Acs Appl Mater Inter* **2022**, *14*, 14654.
[7] B. R. Tian, J. Y. Liu, W. Z. X. Yang, J. B. Wan, *J Agr Food Chem* **2023**, *71*, 1325.
[8] R. S. Andre, R. Schneider, G. R. DeLima, L. Fugikawa-Santos, D. S. Correa, *ACS Sens.* **2024**, *9*, 631.
[9] T. Liu, N. Zheng, Y. M. Ma, Y. Zhang, H. Y. Lei, X. Y. Zhen, Y. Wang, D. X. Gou, J. Zhao, *Int. J. Biol. Macromol.* **2024**, *275*, 133554.
[10] A. Kishore, S. M. Aravind, P. Kumar, A. Singh, K. Kumari, N. Kumar, *Packag Technol Sci* **2024**, *37*, 399.
[11] Y. K. Wang, Z. Y. Jin, Z. J. Zhang, C. K. Zhou, Z. Sun, F. Yan, *Acs Appl Mater Inter* **2023**, *15*, 33998.
[12] R. Merckx, J. Becelaere, E. Schoolaert, O. Frateur, M. N. Leiske, D. Peeters, F. A. Jerca, V. V. Jerca, K. De Clerck, R. Hoogenboom, *Chem. Mater.* **2023**, *35*, 7079.
[13] V. Thakur, B. K. Satapathy, *Acs Food Sci Technol* **2023**, *3*, 2094.
[14] Q. S. Tang, J. W. Hu, S. Li, S. D. Lin, Y. Y. Tu, X. F. Gui, *Int J Food Sci Tech* **2022**, *57*, 6867.
[15] W. Liu, J. Chen, H. Ye, C. Su, Z. Z. Wu, L. Huang, L. Z. Zhou, X. Wei, J. Pang, S. Y. Wu, *Acs Appl Mater Inter* **2024**, *16*, 10785.
[16] S. Sudheer, S. Bandyopadhyay, R. Bhat, *Int. J. Biol. Macromol.* **2023**, *248*, 125845.
[17] Y. Kumar, Y. Bist, D. Thakur, M. Nagar, D. C. Saxena, *Int. J. Biol. Macromol.* **2024**, *276*.
[18] H. D. Hao, B. C. Duan, L. D. Zhang, L. Wang, L. L. Zhang, Y. F. Wang, Y. Y. Li, C. M. Zhao, G. C. Jia, Y. L. Li, C. J. Liu, K. Lu, *Food Biosci* **2024**, *57*, 103474.
[19] D. M. Yang, Q. Liu, X. Zeng, X. T. Chen, M. Li, X. L. Wu, Y. Liu, Y. Z. Zheng, J. H. Xiang, C. C. Wang, W. Y. Weng, Y. C. Zhang, *Int. J. Biol. Macromol.* **2023**, *253*, 127052.
[20] L. Cao, G. Sun, C. Zhang, W. Liu, J. Li, L. Wang, *J Agr Food Chem* **2019**, *67*, 2066.
[21] C. Rukchon, A. Nopwinyuwong, S. Trevanich, T. Jinkarn, P. Suppakul, *Talanta* **2014**, *130*, 547.
[22] M. Tang, J. Z. Song, S. Y. Zhang, X. L. Shu, S. Liu, M. Ashrafizadeh, Y. N. Ertas, Y. Zhou, M. Lei, *J Transl Med* **2024**, *22*, 970.
[23] M. Jahanbakhshi, M. Shahrousvand, *Int. J. Polym. Mater. Polym. Biomater.* **2024**, *73*, 250.
[24] H. Rammal, A. GhavamiNejad, A. Erdem, R. Mbeleck, M. Nematollahi, S. E. Diltemiz, H. Alem, M. A. Darabi, Y. N. Ertas, E. J. Caterson, N. Ashammakhi, *Mater. Chem. Front.* **2021**, *5*, 4368.
[25] T. F. Li, M. Ashrafizadeh, Y. R. Shang, Y. N. Ertas, G. Orive, *Drug Discov Today* **2024**, *29*, 103851.
[26] Z. Wang, S. Pang, X. L. Liu, Z. Dong, Y. Tian, M. Ashrafizadeh, N. Rabiee, Y. N. Ertas, Y. Mao, *Int. J. Biol. Macromol.* **2024**, *273*, 132579.
[27] K. Karimi, S. Mojtabavi, P. M. Tehrany, M. M. Nejad, A. Rezaee, S. Mohtashamian, E. Hamedi, F. Yousefi, F. Salmani, M. A. Zandieh, N. Nabavi, N. Rabiee, Y. N. Ertas, S. Salimimoghadam, M. Rashidi, P. Rahmanian, K. Hushmandi, *Int. J. Biol. Macromol.* **2023**, *242*, 124935.
[28] B. Farasati Far, M. R. Naimi-Jamal, M. Jahanbakhshi, A. Hadizadeh, S. Dehghan, S. Hadizadeh, *Sci. Rep.* **2024**, *14*, 7505.
[29] A. Taheriazam, M. Entezari, Z. M. Firouz, S. Hajimazdarany, M. H. Heydargoy, A. H. A. Moghadassi, A. Moghadaci, A. Sadrani, M. Motahhary, A. H. Nashtifani, A. Zabolian, T. Tabari, M. Hashemi, R. Raesi, M. Jiang, X. Zhang, S. Salimimoghadam, Y. N. Ertas, D. Sun, *Environ. Res.* **2023**, *228*, 115912.
[30] Y. Cheng, B. Farasati Far, M. Jahanbakhshi, S. Bahrami, P. Tamimi, M. Sedaghat, E. Ghazizadeha, *RSC Adv.* **2023**, *13*, 18450.
[31] W. Hu, Z. Wang, Y. Xiao, S. Zhang, J. Wang, *Biomater. Sci.* **2019**, *7*, 843.
[32] B. Farasati Far, M. Jahanbakhshi, L. Jameie, F. Zolfigol, P. Taromi, Y. N. Ertas, *ACS Appl. Polym. Mater* **2024**, *6*, 9545.
[33] F. Mushtaq, Z. A. Raza, S. R. Batool, M. Zahid, O. C. Onder, A. Rafique, M. A. Nazeer, *Int. J. Biol. Macromol.* **2022**, *218*, 601.
[34] B. Farasati Far, M. Omrani, M. R. Naimi Jamal, S. Javanshir, *Commun. Chem.* **2023**, *6*, 28.
[35] P. Dam, S. Shaw, R. Mondal, J. Chakraborty, T. Bhattacharjee, I. K. Sen, S. Manna, A. Sadat, S. Suin, H. Sarkar, Y. N. Ertas, A. K. Mandal, *RSC Adv.* **2024**, *14*, 26723.
[36] S. Bazzazan, K. Moeinabadi-Bidgoli, Z. A. Lalami, S. Bazzazan, M. Mehrarya, F. E. Yeganeh, F. Hejabi, I. Akbarzadeh, H. Noorbazargan, M. Jahanbakhshi, N. Hossein-khannazer, E. Mostafavi, *J. Drug Delivery Sci. Technol.* **2023**, *79*, 104009.
[37] S. H. Lv, S. S. Zhang, J. J. Zuo, S. Liang, J. H. Yang, J. L. Wang, D. Q. Wei, *Int. J. Biol. Macromol.* **2023**, *242*, 124915.
[38] H. Y. Deng, J. Ye, Z. J. Zu, Z. Q. Lin, H. Q. Huang, L. Y. Zhang, X. J. Ye, H. P. Xiang, *Chem. Eng. J.* **2023**, *465*, 143038.
[39] M. Grosjean, L. Gangolphe, B. Nottelet, *Adv. Funct. Mater.* **2023**, *33*, 2205315.
[40] B. Farasati Far, M. R. Naimi-Jamal, M. Jahanbakhshi, S. Keihankhadiv, F. Baradarbarjastehbaf, *Sci. Rep.* **2024**, *14*, 19217.
[41] B. Farasati Far, M. R. Naimi-Jamal, M. Jahanbakhshi, S. A. Khalafvandi, M. Alian, R. Jahromi, *J. Mol. Liq.* **2024**, *395*, 123839.
[42] B. Farasati Far, M. R. Naimi-Jamal, M. Jahanbakhshi, H. Rostamani, M. Karimi, S. Keihankhadiv, *Int. J. Biol. Macromol.* **2023**, *253*, 127448.
[43] L. Liu, A. Shi, S. Guo, Y. e. Fang, S. Chen, J. Li, *React. Funct. Polym.* **2010**, *70*, 301.

[44] T. Brossier, G. Volpi, J. Vasquez-Villegas, N. Petitjean, O. Guillaume, V. Lapinte, S. Blanquer, *Biomacromolecules* **2021**, *22*, 3873.
[45] R. Gupta, S. Swarupa, C. Mayya, D. Bhatia, P. Thareja, *ACS Appl. Bio Mater.* **2023**, *6*, 578.
[46] B. Rostaminejad, A. R. Karimi, M. Dinari, M. Hadizadeh, *ACS Appl. Bio Mater.* **2023**, *6*, 1242.
[47] D. S. Kong, Y. M. Li, B. Yang, Y. K. Pang, H. Yuan, C. Du, Y. Q. Tan, *Small* **2024**, *20*, 2403052.
[48] M. Jridi, S. Hajji, H. B. Ayed, I. Lassoued, A. Mbarek, M. Kammoun, N. Souissi, M. Nasri, *Int. J. Biol. Macromol.* **2014**, *67*, 373.
[49] S. Chatterjee, K. Ghosal, M. Kumar, S. Mahmood, S. Thomas, *J. Drug Delivery Sci. Technol.* **2023**, *79*, 104095.
[50] M. Omrani, M. R. Naimi-Jamal, B. F. Far, *Carbohydr. Polym.* **2022**, *298*, 120143.
[51] M. Nami, M. Taheri, J. Siddiqui, I. A. Deen, M. Packirisamy, M. J. Deen, *Adv. Mater. Technol.* **2024**, *9*, 2301347.
[52] D. Kim, S. Lee, K. Lee, S. Baek, J. Seo, *Food Sci. Biotechnol.* **2017**, *26*, 37.
[53] P. Lu, Y. Yang, R. Liu, X. Liu, J. Ma, M. Wu, S. Wang, *Carbohydr. Polym.* **2020**, *249*, 116831.
[54] B. Veltman, D. Harpaz, Y. Cohen, E. Poverenov, E. Eltzov, *Int. J. Biol. Macromol.* **2022**, *194*, 666.
[55] I. J. Budiarso, N. D. W. Rini, A. Tsalsabila, M. D. Birowosuto, A. Wibowo, *ACS Biomater. Sci. Eng.* **2023**, *9*, 3084.